Highlights

Heat Capacity of Liquid Transition Metals Obtained with Aerodynamic Levitation

Yifan Sun, Hiroaki Muta, Yuji Ohishi

- This study utilizes the newly developed “multiple-gas cooling” method
- The method is used in conjunction with aerodynamic levitation
- The approach can measure the heat capacity of transition metals up to 3000 K
- This study also compares and reviews the heat capacity of various transition metals

Heat Capacity of Liquid Transition Metals Obtained with Aerodynamic Levitation

Yifan Sun[a,*], Hiroaki Muta[a], Yuji Ohishi[a]

[a]*Graduate School of Engineering, Osaka University, Yamadaoka 2-1, Suita, 565-0871, Osaka, Japan*

Abstract

The development of contactless measurement methods has allowed investigating the properties of molten materials at high temperatures in a controlled environment. As the sample is not in contact with any container walls while being heated, levitation techniques have an edge over traditional contact methods at elevated temperatures. Among the various thermophysical properties of interest, it has been challenging to measure heat capacity with levitation techniques because it is directly related to the emissivity of the sample. Previous studies on heat capacity measurement with various levitation techniques have produced results with large deviations, especially at elevated temperatures. In addition, there is a general lack of information on the heat capacity of liquid transition metals at temperatures exceeding 2000 K, especially using conventional calorimetry methods. In this study, we successfully obtained the isobaric heat capacity of liquid transition metals such as Co, Hf, Ir, Mo, Nb, Rh, Ru, Ti, V, and Zr with aerodynamic levitation using the newly developed "multiple-gas cooling" method. A comparison between our reported values and reference data enabled us to assess the accuracy of previous experiments and provide much needed heat capacity data for high-temperature liquid metals. This study highlights the applicability and reliability of the multiple-gas cooling method for measuring the heat capacity of liquid non-noble metals at temperatures approaching 3000 K.

Keywords: Liquid metals, Transition metals, High-temperature, Heat capacity, Aerodynamic levitation

1. Introduction

Heat capacity is a key parameter in the study of thermodynamics because it is connected to a system's internal energy, enthalpy, entropy, and Gibbs free energy [1]. From the second law of thermodynamics, we know that heat transfer occurs when there is a temperature difference, and heat capacity is involved in this process. In metalworking, the solidification time is directly related to the heat capacity of the cast metal according to Chvorinov's rule [2]. In heat storage/heat shielding designs, heat capacity determines how much energy the system can store or release within the allowed temperature range [3, 4].

Various methods for measuring the heat capacity of liquid materials at high temperatures have been developed over the decades. Drop calorimetry methods have been used to determine the heat

*Corresponding author

Email address: yifansun2016@ms.see.eng.osaka-u.ac.jp (Yifan Sun)

capacity of both solids and liquids [5, 6, 7, 8], and J. A. Treverton & J. L. Margrave incorporated electromagnetic levitation (EML) with drop calorimetry into levitation calorimetry [9, 10, 11]. To prevent sample contamination, the pulse heating method was used by J. L. Margrave [11] and Pottlacher et al. [12, 13, 14, 15, 16] to obtain various thermophysical properties such as the density, enthalpy, and heat capacity of liquid metals. Paradis et al. [17, 18, 19, 20, 21, 22, 23] used electrostatic levitation (ESL) to analyze the cooling curve of a levitated molten sample to derive the ratio of heat capacity to emissivity. By assuming wavelength-independent emissivity values, Paradis et al. converted the ratio into heat capacity. More recently, to correct for the uncertainty in assuming a constant emissivity across all wavelengths, Ishikawa et al. [24, 25, 26, 27, 28, 29] used a blackbody furnace (BBF) setup to determine the emissivity of the sample for use in heat capacity calculations. A BBF was also used with EML by Kobatake et al. [30, 31], and Watanabe et al. [32, 33] to determine the heat capacity with laser modulation calorimetry. Among these methods used in heat capacity measurements, ESL + BBF is one of the more accurate methods because this approach includes few sources of error. The contactless vacuum environment prevents the high-temperatures reactive liquid metals from reacting with the measurement apparatus or gases. The heat loss analysis of the levitated spherical sample is straightforward, as only radiative heat loss occurs under high vacuum.

However, although the measurement methods mentioned above are frequently used to study liquid metals and alloys, they are not generally used for liquid oxides. This is because EML-related methods and the pulse heating technique require samples that are good conductors. For ESL, levitation of liquid oxides is also challenging under 1-G conditions, and microgravity is currently used to help study liquid oxides [34]. Because of this lack of heat capacity measurement methods for liquid oxides, we introduced the "multiple-gas cooling" method [35] for aerodynamic levitation (ADL). ADL uses gas to levitate samples and can stably levitate liquid oxides under 1-G conditions. However, the heat loss of a sample levitated with ADL is more complicated than that in the case of ESL because convective heat loss is present. To calibrate our heat loss model for ADL, we utilized the heat capacity and emissivity values reported using ESL + BBF by Ishikawa et al [28]. The reported heat capacity values for Au, Cu, Fe, Ni, and Pd measured with the multiple-gas cooling method agreed well with the reference values. However, these metals are rather stable, do not readily form oxides at high temperatures based on the Ellingham diagram, and have melting points lower than 2000 K. In order to use the multiple-gas cooling method to measure the heat capacity of most liquid metal oxides, such as Al_2O_3, ZrO_2, and lanthanide oxides, with melting points exceeding 2000 K, the accuracy of the multiple-gas cooling method at higher temperatures must be determined.

Thus, the focus of this study was to assess the multiple-gas cooling method's accuracy at higher temperatures by comparing the obtained data with those provided by ESL + BBF. Liquid transition metals are ideal targets for this study according to the previous findings of Ishikawa et al., who reported the heat capacity of several transition metals [24, 25, 26, 27, 28, 29] with melting points over 2000 K. In addition, the reported heat capacity values in the present study can fill the gaps in existing literature. There is still no consensus on the heat capacities of various transition metals because their high melting points have resulted in either a lack of reported values or noticeable scattering in reference data. Transition metals are some of the most industrially important materials because of their excellent physical properties, such as high tensile strength, high corrosion resistance, and high melting temperatures. Accurate information on the heat capacity of pure transition metals will contribute to not only future discussions on the mixing behaviors of these metals but also controlling the casting process as well as designing new alloys.

In this article, we first discuss the aerodynamic levitation setup used in our experiments. The

heat loss models used to calculate the radiative and convection heat loss are then introduced. To correct for the levitation nozzle's conical shape, a calibration process using a material, in this case platinum, with known emissivity and heat capacity is conducted. The measured heat capacity data of liquid transition metals, Co, Hf, Ir, Mo, Nb, Rh, Ru, Ti, V, and Zr, are presented in the results and discussion section and compared with previously published results.

2. Experiment method

2.1. Experiment setup

The ADL setup used in this study was based on the designs of Langstaff et al. [36] and Kargl et al. [37]. A detailed description of the current ADL setup has been presented in our previously published articles [35, 38]; thus, only a brief description of the key components is provided here. The 3D renderings of the overall ADL setup and the levitation nozzle used in this study are shown in Figs.1,2. Some components of the aerodynamic levitator were omitted to make the figure more comprehensible. As shown in Fig.1, two 976 nm fiber lasers (pearl, nLight) were used to heat the sample from the top and bottom. A sapphire window and a 1400 nm longpass filter (FEL1400, Thorlabs) were placed in front of the pyrometer (1.55 μm, CHINO) to block unwanted reflection from the fiber lasers. Another set of sapphire windows and a 550 nm short pass filter (FESH550, Thorlabs) was placed in front of the CCD camera for sample observations at high temperatures. The 3D rendering of the 1.4-mm-diameter conical nozzle used for levitation is shown in Fig.2. During the experiment, cooling water was constantly circulated around the copper nozzle to keep it between 25°C and 27°C. Levitation gas was introduced into the nozzle through a 3-mm-diameter hole on the nozzle wall. In this study, high-purity argon (5N, Air Liquide) and krypton (5N, Tokyo Gas Chemicals) gases were used for heat capacity measurements, and an Ar-4%H_2 mixture (Air Liquide) was used to make and reduce the samples. In this study, oxidation was minimized by placing a sapphire top cover over the nozzle.

2.2. Temperature calibration

The pyrometer treats the sample as a blackbody (ϵ=1), which requires the collected temperature data to be corrected using the material's melting point and a derivation based on Wien's law [39]:

$$\frac{1}{T} - \frac{1}{T_P} = \frac{1}{T_L} - \frac{1}{T_{P,L}} \tag{1}$$

Here, T is the corrected temperature, T_P is the temperature recorded by the pyrometer, T_L is the melting point of the sample, and T_P, L is the as-recorded melting temperature of the sample. $T_{P,L}$ can be identified by a sudden increase in the temperature after recalescence. A comparison between the as-recorded and corrected temperature curves for liquid cobalt is shown in Fig.3. During this temperature correction process, we assumed that the emissivity of the sample in the liquid phase is constant and equal to that at the melting point of the sample, which is a reasonable assumption for liquid metals [40]. However, to minimize the effect of temperature on the emissivity of the sample, the reported heat capacity values are confined to ± 50 K around the melting point of the material. The cooling curves of each material cooled in argon and krypton after correction based on their respective melting points are shown in Fig.A.5.

2.3. Heat loss calculations

In ADL, a levitated spherical sample experiences a total heat loss comprising radiation heat loss to the surrounding environment and forced convection heat loss to the levitation gas. The contribution of radiation heat loss q_{Rad} can be described by the Stefan–Boltzmann law:

$$q_{Rad} = A\epsilon\sigma T^4 \tag{2}$$

where A is the sample's surface area, ϵ is the emissivity of the sample, σ is the Stefan–Boltzmann constant, and T is the temperature of the sample. The contribution of convection heat loss q_{Conv} can be expressed based on Newton's law of cooling:

$$q_{Conv} = hA(T - T_{gas}) \tag{3}$$

where h is the heat transfer coefficient, A is the surface area of the sample, T is the temperature of the sample, and T_{gas} is the temperature of the levitation gas, which is assumed to be constant at 25°C.

The heat transfer coefficient h can be expressed using Ranz-Marshall's equation [41], which originally describes the convection heat loss of a falling droplet in an open environment. For $0.6 < Pr < 380, 1 < Re < 10^5$,

$$h = \frac{\kappa}{d} \times (2 + 0.6Re^{\frac{1}{2}}Pr^{\frac{1}{3}}) \tag{4}$$

Here, κ is the thermal conductivity of the gas, Re is the Reynolds number, and Pr is the Prandtl number. To calculate the Reynolds number, it is necessary to know the relative velocity of the sample relative to the levitation gas. In this study, we assumed this velocity difference to be the terminal velocity of the sample, which can be derived by considering the combined effect of gravity, drag, and buoyancy,

$$v = \frac{4}{3 \times C_d}\frac{\rho_s - \rho_f}{\rho_f}d^{\frac{1}{2}} \tag{5}$$

Here, ρ_s is the density of the sample, ρ_f is the density of the levitation gas, and d is the diameter of the levitated sample, and C_d is the drag coefficient. The ranges of the Reynolds numbers for each material used in this study are listed in Tab.1. For Reynolds numbers higher than 500, the drag coefficient is approximately 0.44 [42].

C. Tackes [43] incorporated the unmodified Ranz-Marshall equation to describe the convective heat loss of a falling sample in levitation drop calorimetry measurements. In this study, we modified the Ranz-Marshall equation (Eq.4) because the levitated sample is semi-confined within a conical nozzle and not in an open environment. However, a detailed analysis of how the Ranz-Marshall equation should be modified for a droplet in a conical nozzle at a low gas flow rate is currently not available. Previous studies [44, 45, 46, 47, 48, 49, 50, 51] have multiplied additional terms with the Ranz-Marshall equation to correct for the steep temperature gradient (plasma heating involved), but these modifications do not apply to the current situation. In this study, we introduced an extra dimensionless coefficient α, and therefore, the modified Ranz-Marshall equation is expressed as

$$h = \alpha \times \frac{\kappa}{d} \times (2 + 0.6Re^{\frac{1}{2}}Pr^{\frac{1}{3}}) \tag{6}$$

We assumed that α should be related to the type of gas used as well as the diameter of the levitated sample. Therefore, it is necessary to locate the diameter range of the sample that has the least effect on the value of α. Under an ideal scenario, Eq.6 reverts back to Eq.4, where $\alpha = 1$.

Material	Reynolds numbers	
	Ar	Kr
Co	1250– 1690	1620 – 2210
Hf	1410 – 1810	1850 – 2370
Ir	2060 – 2600	2690 – 3400
Mo	1270 – 1460	1660 – 1900
Nb	1190 – 1510	1560 – 1980
Rh	1390 – 1670	1820 – 2190
Ru	1610 – 1720	2100 – 2250
Ti	930 – 1220	1220 – 1600
V	1150 – 1410	1510 – 1840
Zr	1040 – 1310	1370 – 1720

Table 1: Calculated range of the Reynolds numbers for each material used in this study.

In summary, the total heat loss q at a specific temperature can be expressed as follows:

$$q = A\epsilon\sigma T^4 + \frac{A\alpha\kappa}{d}(2 + 0.6Re^{\frac{1}{2}}Pr^{\frac{1}{3}})(T - T_{gas}) \tag{7}$$

A detailed discussion on the heat loss model used in this study can be found in our previous publication [35].

2.4. Heat capacity calculation and calibration

The heat loss of the sample at a specific temperature T over an infinitesimal duration Δt can be expressed as

$$q\Delta t = [A\epsilon\sigma T^4 + Ah(T - T_{gas})]\Delta t \tag{8}$$

This can be further transformed by incorporating the sample mass m, heat capacity C_P, and temperature change ΔT into

$$mC_P\Delta T = [A\epsilon\sigma T^4 + A\alpha h(T - T_{gas})]\Delta t \tag{9}$$

$$\frac{dT}{dt} = \frac{A}{mC_P}[\epsilon\sigma T^4 + \alpha h(T - T_{gas})] \tag{10}$$

In this study, two types of levitation gas were used. Therefore, for the same sample, Eq.10 holds true for each type of levitation gas:

$$\frac{dT_{inAr}}{dt} = \frac{A}{mC_P}[\epsilon\sigma T_{inAr}^4 + \alpha_{Ar}h(T_{inAr} - T_{gas})] \tag{11}$$

$$\frac{dT_{inKr}}{dt} = \frac{A}{mC_P}[\epsilon\sigma T_{inKr}^4 + \alpha_{Kr}h(T_{inKr} - T_{gas})] \tag{12}$$

Here, T_{inAr} and T_{inKr} denote the temperatures of the sample in argon and krypton gas, respectively. As mentioned previously, the introduced α coefficient is assumed to be dependent on the gas type; therefore, α_{Ar} and α_{Kr} are used above. T_{gas} is the temperature of the levitation gas. Each of the experimentally obtained cooling curves, $\frac{dT}{dt}$, is related to three unknown variables (C_P, ϵ, and α), and two sets of cooling curves are not sufficient to generate a unique solution. Therefore, the values of α should be defined first.

To determine α_{Ar} and α_{Kr} in Eqs.11,12, the $\frac{dT}{dt}$ term (cooling curves), emissivity, and heat capacity of a specific material must be known. In this study, platinum was used to calibrate the α coefficients because platinum is inert, even at high temperatures. The cooling curves of liquid platinum in argon and krypton gas were first obtained using ADL. For liquid platinum, an emissivity value of 0.25 and a heat capacity value of 38.8±1.8 J/molK at the melting point, as reported by Ishikawa et al. [29], were used for calibration. This specific study by Ishikawa et al. was selected because ESL + BBF can produce highly reliable heat capacity data concerning liquid metals. This is because the sample is measured under high-vacuum conditions with electrostatic levitation; the only source of heat loss is radiation heat loss, which can be directly calculated using the Stefan–Boltzmann law. The high-vacuum and contactless conditions also ensure that the sample's surface condition remains constant during the heat capacity measurements. In addition, the use of a blackbody furnace for emissivity measurement is most suited for ESL because the sample can be assumed to be perfectly spherical. α_{Ar} and α_{Kr} can be obtained by performing least-squares fitting of the right-hand sides of Eqs.11,12 to the experimentally obtained cooling curves.

As mentioned in our previous report [35], the α coefficient is least sensitive to changes in the sample diameter when the diameter is between 1.2 and 1.6 mm. No changes were made to the nozzle; therefore, this range should still hold. In this study, three platinum samples with diameters within this range were used at the melting point for calibration, and the obtained α coefficients were $\alpha_{Ar} = 0.750 \pm 0.053$, $\alpha_{Kr} = 0.783 \pm 0.068$. Compared to the α values used in our previous experiment, the difference was less than 1%. Using these α values, we can evaluate how well the heat loss model developed in this study can describe the cooling curve of a levitated droplet around its melting point in ADL using Eqs.11,12. An example is presented in Fig.4 for a liquid cobalt sample cooled in argon and krypton gas. The radiation heat loss contribution was calculated using the Stefan–Boltzmann law, and the convective heat loss contribution was calculated using the modified Ranz-Marshall equation. As we can see, the experimental cooling curve of liquid cobalt within 50 K of its melting point can be well described by the heat loss model used in this study. Although the sample's emissivities can also be obtained from Eqs.11,12, these values are not reported here because emissivity is highly sensitive to the sample's surface conditions. Heat capacity, on the other hand, is the sample's bulk property. Therefore, the high-vacuum condition used in ESL + BBF experiments is more suitable for measuring liquid metal's emissivity.

3. Results and Discussion

3.1. Sample preparation

Detailed information on the transition metals used in this study is presented in Tab.2. Hafnium and zirconium have similar properties, and one is generally present in small amounts as impurities. Based on the Hf-Zr binary phase diagrams [52], after solidification, the Zr-Hf solid solution (Hf-rich side) transforms from BCC to HCP, which can explain why the cooling curve of hafnium in Fig.A.5 contains two recalescence regions. The same phase transformation takes place for the Zr-rich side at a much lower temperature, which is why this transition is not visible in the cooling curves of zirconium shown in Fig.A.5.

As mentioned previously, with the current setup, the introduced coefficients α_{Ar} and α_{Kr} that modify the convection heat loss are the least sensitive to changes in the sample diameter when the sample diameter is between 1.2 to 1.6 mm. To satisfy this condition, the mass of the sample

Chemical Name	Purity	Source
Co	0.9997	Rare Metallic
Hf	0.999 (Zr≤0.03wt)	Furuuchi Chemical
Ir	0.999	Nilaco
Mo	0.9995	Nilaco
Nb	0.999	Nilaco
Ti	0.999	Furuuchi Chemical
Rh	0.999	Nilaco
Ru	0.9995	Rare Metallic
V	0.999	Furuuchi Chemical
Zr	0.999 (Hf≤35ppm)	Rare Metallic

Table 2: List of chemicals used in this study.

was controlled so that at the melting point, the sample diameter was within 1.2 and 1.6 mm. The samples were prepared under an Ar-4%H_2 environment and then subjected to measurements using argon gas. After cooling and before measurements with krypton gas, the sample was cleaned with an Ar-4%H_2 mixture. This is to ensure that the surface conditions of the sample before cooling in argon and krypton gas are the same.

The average changes in the sample mass are listed in Tab.3. An average mass change of less than 1% was observed across all samples. From these negligible mass changes, we can confirm that the added top sapphire window cover was effective in preventing sample oxidation. As shown in Tab.3, rhodium has the greatest mass decrease because one of the rhodium samples experienced a mass decrease of approximately -2% owing to sample evaporation.

Material	Average mass change (%)
Co	-0.32
Hf	+0.22
Ir	-0.02
Mo	-0.37
Nb	+0.03
Ti	+0.39
Rh	-0.65
Ru	-0.01
V	+0.37
Zr	+0.23

Table 3: Average change in sample mass before and after measurement.

3.2. Heat capacity of liquid transition metals

The heat capacity data for various transition metals obtained using the multiple-gas cooling method and the corresponding standard errors are listed in Tab.4. Five samples were measured for each material, except for molybdenum. Molybdenum samples were difficult to prepare as it has the highest melting point among the materials reported in this study. Therefore, only four spherical molybdenum samples were successfully fabricated. Our data agree well with these

listed values from literature, except for liquid ruthenium, because of the scarcity of available data [19, 53].

Material (T_m)	Cp (J/mol K)	Reference	Comment
Co (1768 K)	44.3±0.9	This study	ADL
	40.6	Wang et al. [54]	Levitation drop calorimetry
	41.2	Watanabe et al. [32]	Levitation laser modulation
	45.9	Hess et al. [55]	Pulse heating
	48.5±0.8	J. A. Treverton and J. L. Margrave [10]	Levitation drop calorimetry
	50.2	J. L. Margrave [11]	Levitation drop calorimetry
Hf (2506 K)	38.1±0.8	This study	ADL
	33.5	Paradis et al. [18]	ESL
	41.9	Korobenko et al. [56]	Pulse heating
	44.8	Kang et al. [57]	ESL + solid Hf emissivity
	60.32	Kang et al. [57]	ESL
Ir (2719 K)	45.1±1.4	This study	ADL
	30.1	J. L. Margrave [11]	Pulse heating
	34.3	Paradis et al. [19]	ESL
	44.2	C. Cagran and G. Pottlacher [58]	Pulse heating
	59.4	J. L. Margrave [11]	Levitation drop calorimetry
Mo (2896 K)	41.5±0.7	This study	ADL
	34.2	Paradis et al. [20]	ESL
	37.7	J. L. Margrave [11]	Levitation drop calorimetry
	40.7	Minakov et al. [59]	Simulation
	47.2	Cagran et al. [60]	Pulse heating
	53.7	Pottlacher et al. [13]	Pulse heating
Nb (2750 K)	42.3±1.8	This study	ADL
	38.9	K. Boboridis [61]	Pulse heating
	40.6	J. L. Margrave [11]	Levitation drop calorimetry
	40.6	Paradis et al. [21]	ESL
	40.8	A. Cezairliyan and J. L. McClure [62]	Pulse heating
	41.9	Ishikawa et al. [26]	ESL + blackbody furnace
	45.7	Kang et al. [57]	ESL
Rh (2237 K)	39.8±1.1	This study	ADL
	32.2	Paradis et al. [19]	ESL
	34.8	Kang et al. [57]	ESL
	41.8	Ishikawa et al. [27]	ESL + blackbody furnace
	46.1	Hupf et al [14].	Pulse heating
Ru (2607 K)	46.4±0.9	This study	ADL
	35.9	Paradis et al. [19]	ESL
	41.9	Barin et al. [53]	Recommended value
Ti (1941 K)	44.4±0.7	This study	ADL
	35.3	K. Boboridis [61]	Pulse heating
	42.7	Kang et al. [57]	ESL
	43.4	J. L. Margrave [11]	Levitation drop calorimetry
	44.9	Ishikawa et al. [25]	ESL + blackbody furnace
	45.5	P-F. Paradis and W-K. Rhim [22]	ESL
	48.9	Watanabe et al. [33]	Levitation laser modulation
	49.9	Wilthan et al. [63]	Pulse heating
V (2183 K)	48.0±1.4	This study	ADL
	46.9	J. L. Margrave [11]	Levitation drop calorimetry
	47.3	J. L. Margrave [11]	Pulse heating
	48.5	Ishikawa et al. [24]	ESL + blackbody furnace
	48.8	Paradis et al. [17]	ESL
	49.1	Pottlacher et al. [12]	Pulse heating
Zr (2128 K)	38.9±0.7	This study	ADL
	39.1	Kang et al. [57]	ESL
	39.7	P-F. Paradis and W-K. Rhim [23]	ESL
	40.6	J. L. Margrave [11]	Levitation drop calorimetry
	40.9	Ishikawa et al. [28]	ESL + blackbody furnace
	45.3	Brunner et al. [64]	Pulse heating

Table 4: Heat capacity values of liquid transition metals obtained with aerodynamic levitation and a summary of values from literature.

The heat capacity values of various molten metals have been reported by Paradis et al.

[17, 18, 19, 20, 21, 22, 23] through analyzing the samples' cooling curves obtained with ESL. However, because the hemispherical emissivity of most liquid metals was not known at that time, when calculating the heat capacity, Paradis et al. assumed a wavelength-independent emissivity value [17, 18, 19, 20, 21, 22, 23]. T. Ishikawa, who worked closely with P-F. Paradis on the development of ESL in the Japan Aerospace Exploration Agency (JAXA), solved the unknown emissivity issue by using a blackbody furnace to aid in the measurement of the hemispherical emissivity of the levitated sample [28]. Although the values reported by these two researchers are, for most liquid metals, in good agreement, Ishikawa et al. [24, 25, 26, 27, 28, 29] could provide heat capacity data with greater accuracy by incorporating the measured hemispherical emissivity in radiative heat loss analysis instead of assuming emissivity to be wavelength independent. Because the multiple-gas cooling method is calibrated based on the results of the ESL + BBF method, we expect good agreement between the calculated heat capacity values obtained with these two methods. By comparing our reported heat capacity values with those by Ishikawa et al. [24, 25, 26, 27, 28] on liquid V, Ti, Nb, Rh, and Zr, we calculated the maximum deviation in the average heat capacity value to be approximately 5%, for both liquid Rh and Zr. For the heat capacities of liquid Nb, Ti, and V, the deviations are approximately 1% between the two methods. As compared with the degree of deviations in case of other references, results obtained in this study are generally in accord with the results by Ishikawa et al. This agreement shows that the accuracy of the multiple-gas cooling method is not lost when applied to measurements at much higher temperatures. Therefore, we reckon that our reported heat capacity data for liquid transition metals that have not previously had data reported using ESL + BBF, such as Co, Hf, and so on, are reliable.

Kang et al. [57] also used ESL, but with a different approach to heat capacity analysis. Because the heterogeneous nucleation of the sample can be prevented in a high-vacuum containerless environment, they first obtained the hypercooling limit (T_{hyp}) of various metals. Then, using the literature heat of fusion values (ΔH_f), they calculated the heat capacity based on $\Delta H_f = T_{hyp} C_P$. Therefore, the accuracy of the obtained heat capacity depends on that of the determined hypercooling limits and the reported heat of fusion data. While the values reported by Kang et al. are generally in good agreement with those reported in this study and by Ishikawa et al., the heat capacity of liquid hafnium showed a significant deviation (~20 J/mol K). The authors attributed this deviation to the use of inaccurate heat of fusion [65] and attempted calculations with the emissivity of solid hafnium [65]. Although this provided a more reasonable value of 44.8 J/mol K, the uncertainty introduced when using the emissivity of the solid is unknown.

For all the heat capacity measurement methods shown in Tab.4, developments in image recording, temperature calibration, and data processing all affect the obtained results to some extent. Perhaps the impact is most significant for pulse heating experiments because the measurement is completed in less than 100 μs; therefore, ultra-fast data recording systems are essential for providing accurate results. This could be seen in how some of the earlier data reported by Margrave et al. (e.g., liquid Ir [11]) and Pottlacher et al. (e.g., liquid Mo [13]) differ from other values from literature. Finally, our data agree well with the levitation drop calorimetry results obtained by J. A. Treverton and J. L. Margrave [10, 11], except for liquid iridium. The heat capacity of liquid iridium reported by J. L. Margrave is much higher than those reported in the literature, which could have resulted from difficulties in obtaining accurate temperature data at high temperatures, one of the major sources of error, as mentioned by the author [11].

4. Conclusion

In this study, we used a novel multiple-gas cooling method developed for ADL to measure the heat capacity of various liquid transition metals (Co, Hf, Ir, Mo, Nb, Rh, Ru, Ti, V, and Zr) around their melting points. As this measurement method is based on aerodynamic levitation, it is difficult to perform experiments on materials with high vapor pressure or high oxygen affinity. Additionally, the sapphire top cover is not completely transparent to the heating laser, thus limiting the current measurement to liquid metals with melting points lower than 3000 K (Re, Ta, and W are therefore not included in this study). A comparison and review of the heat capacity of liquid transition metals is also provided. The results obtained in this study generally agree well with published data, which further confirms the reliability of the multiple-gas cooling method for heat capacity measurements and its applicability at temperatures approaching 3000 K. The current maximum temperature of 3000 K allows for heat capacity measurements for a majority of liquid metal alloys and, more importantly, liquid oxides. For measurements of liquid metals, pure Ar and Kr levitation gases can be used to provide an inert atmosphere. However, for measurements of liquid oxides, gas mixtures containing oxygen must be used to prevent sample reduction. Expressing the thermophysical properties (thermal conductivity, heat capacity, and viscosity) of binary gas mixtures in our ADL setup, which will allow us to correctly model the convection heat loss of the sample, remains a topic for future studies.

Acknowledgment

The authors would like to thank Prof. Ishikawa of the Japan Aerospace Exploration Agency (JAXA) for his constructive criticism of the manuscript. This study was supported by the Japan Atomic Energy Agency Nuclear Energy S&T and Human Resource Development Project through concentrating wisdom Grant Number JPJA18B18071972, a Grant-in-Aid from a fellowship from the Japan Society for the Promotion of Science (JSPS) [20J10376], and JSPS KAKENHI Grant Number JP19K05332.

Competing Interests Statement

The authors declare that they have no competing interests.

Data Availability

The data that support the findings of this study are available from the corresponding author, Y. Sun, upon reasonable request.

References

[1] R. T. DeHoff, Thermodynamic Variables and Relations, 2nd Edition, CRC Press, 2006.
[2] N. Chvorinov, Theory of the solidification of castings, Giesserei 27 (1940) 177–186, 201–208, and 222–225.
[3] I. Sarbu, C. Sebarchievici, A comprehensive review of thermal energy storage, Sustainability 10 (2018) 191–222.
[4] H. P. Garg, S. C. Mullick, A. K. Bhargava, Sensible Heat Storage, Springer, Dordrecht, 1985.
[5] W. T. Thompson, S. N. Flengas, Drop calorimetric measurements on some chlorides, sulfides, and binary melts, Can. J. Chem. 49 (1970) 1550–1563.
[6] K. Yamaguchi, K. Itagaki, Measurement of high temperature heat content of silicon by drop calorimetry, J. Therm. Anal. Calorim. 69 (2002) 1059–1066.

[7] S.V.Stankus, I. Savchenko, O. Yatsuk, A high-temperature drop calorimeter for studying substances and materials in the solid and liquid states, Instrum. Exp. Tech. 60 (2017) 608–613.
[8] M. Hoch, H. L. Johnston, A high temperature drop calorimeter. the heat capacities of tantalum and tungsten between 1000° and 3000°k.1, J. Phys. Chem. 65 (1961) 855–860.
[9] J. A. Treverton, J. L. Margrave, Levitation calorimetry. iii. the enthalpies of fusion and heat capacities for the liquid phases of iron, titanium, and vanadium, J. Chem. Thermodyn. 3 (1971) 473–481.
[10] J. A. Treverton, J. L. Margrave, Levitation calorimetry. iv. the thermodynamic properties of liquid cobalt and palladium, J. Phys. Chem. 75 (1971) 3737–3740.
[11] J. L. Margrave, Determination of thermophysical properties of liquid metals at high temperatures by levitation methods, Mater. Sci. Eng. A 178 (1994) 83–88.
[12] G. Pottlacher, T. Hupf, B. Wilthan, C. Cagran, Thermophysical data of liquid vanadium, Thermochim. Acta 461 (2007) 88–95.
[13] G. Pottlacher, E. Kaschnitz, H. Jager, High-pressure, high-temperature thermophysical measurements on molybdenum, J. Phys.: Condens. Matter 3 (1991) 5783–5792.
[14] T. Hupf, C. Cagran, B. Wilthan, G. Pottlacher, Thermophysical properties of rhodium obtained by fast pulse-heating, J. Phys.: Condens. Matter 21 (2009) 125701.
[15] C. Cagran, G. Pottlacher, Thermophysical properties of palladium, Platinum Metals Rev. 50 (2006) 144–149.
[16] M. Leitner, T. Leitner, A. Schmon, K. Aziz, G. Pottlacher, Thermophysical properties of liquid aluminum, Metall. Mater. Trans. A 48 (2017) 3036–3045.
[17] P. F. Paradis, T. Ishikawa, T. Aoyama, S. Yoda, Thermophysical properties of vanadium at high temperature measured with an electrostatic levitation furnace, J. Chem. Thermodyn. 34 (2002) 1929–1942.
[18] P. F. Paradis, T. Ishikawa, S. Yoda, Non-contact measurements of the thermophysical properties of hafnium-3 mass% zirconium at high temperature, Int. J. Thermophys. 24 (2003) 239–258.
[19] P. F. Paradis, T. Ishikawa, S. Yoda, Ground-based thermophysical property measurements of supercooled and liquid platinum-group metals by electrostatic levitation, Microgravity Sci. Technol. 16 (2005) 94–98.
[20] P. F. Paradis, T. Ishikawa, S. Yoda, Noncontact measurements of thermophysical properties of molybdenum at high temperatures, Int. J. Thermophys. 23 (2002) 555–569.
[21] P. F. Paradis, T. Ishikawa, S. Yoda, Non-contact measurements of thermophysical properties of niobium at high temperature, J. Mater. Sci. 36 (2001) 5125–5130.
[22] P. F. Paradis, W. K. Rhim, Non-contact measurements of thermophysical properties of titanium at high temperature, J. Chem. Thermodyn. 32 (2000) 123–133.
[23] P. F. Paradis, W. K. Rhim, Thermophysical properties of zirconium at high temperature, J. Mater. Res. 14 (1999) 3717–3719.
[24] T. Ishikawa, C. Koyama, Y. Nakata, Y. Watanabe, P.-F. Paradis, Spectral emissivity, hemispherical total emissivity, and constant pressure heat capacity of liquid vanadium measured by an electrostatic levitator, J. Chem. Thermodyn. 163 (2021) 106598.
[25] T. Ishikawa, C. Koyama, Y. Nakata, Y. Watanabe, P. Paradis, Spectral emissivity and constant pressure heat capacity of liquid titanium measured by an electrostatic levitator, J. Chem. Thermodyn. 131 (2019) 557–562.
[26] K. Sakata, Y. Watanabe, J. Okada, M. Kumar, P.-F. Paradis, T. Ishikawa, Ft-ir emissivity measurements of nb melt using an electrostatic levitation furnace, J. Chem. Thermodyn. 91 (2015) 116–120.
[27] T. Ishikawa, J. T. Okada, P. F. Paradis, Y. Watanabe, Spectral emissivity and constant pressure heat capacity of molten nickel and rhodium measured by spectrometers combined with an electrostatic levitator, J. Chem. Thermodyn. 103 (2016) 107–114.
[28] T. Ishikawa, Y. Ito, J. T. Okada, P.-F. Paradis, Y. Watanabe, T. Masaki, Spectral emissivity measurements of liquid refractory metals by spectrometers combined with an electrostatic levitator, Meas. Sci. Technol. 23 (2012) 125602.
[29] T. Ishikawa, J. T. Okada, P.-F. Paradis, Y. Watanabe, Measurement of spectral emissivity and constant pressure heat capacity of liquid platinum with an electrostatic levitator, J. Chem. Thermodynamics. 112 (2017) 7–12.
[30] H. Kobatake, H. Fukuyama, I. Minato, T. Tsukada, S. Awaji, Noncontact modulated laser calorimetry of liquid silicon in a static magnetic field, J. Appl. Phys. 104 (2008).
[31] H. Kawamura, H. Fukuyama, M. Watanabe, T. Hibiya, Normal spectral emissivity of undercooled liquid silicon, Meas. Sci. Technol. 16 (2005) 386–393.
[32] M. Watanabe, J. Takano, M. Adachi, M. Uchikoshi, H. Fukuyama, Thermophysical properties of liquid co measured by electromagnetic levitation technique in a static magnetic field, J. Chem. Thermodyn 121 (2018) 145–152.
[33] M. Watanabe, M. Adachi, H. Fukuyama, Heat capacities and thermal conductivities of palladium and titanium melts and correlation between thermal diffusivity and density of states for transition metals in a liquid state, J. Mol. Liq. 324 (2021) 115138.
[34] C. Koyama, T. Ishikawa, H. Oda, H. Saruwatari, S. Ueno, M. Oshio, Y. Watanabe, Y. Nakata, Densities of liquid lanthanoid sesquioxides measured with the electrostatic levitation furnace in the iss, Journal of the American Ceramic Society 104 (7) (2021) 2913–2918.

[35] Y. Sun, H. Muta, Y. Ohishi, Multiple-gas cooling method for constant-pressure heat capacity measurement of liquid metals using aerodynamic levitator, Rev. Sci. Instrum. 92 (2021) 095102.
[36] D. Langstaff, M. Gunn, G. N. Greaves, A. Marsing, F. Kargl, Aerodynamic levitator furnace for measuring thermophysical properties of refractory liquids, Rev. Sci. Instrum. 84, 124901 (2013).
[37] F. Kargl, C. Yuan, G. N. Greaves, Aerodynamic levitation: thermophysical property measurements of liquid oxides, Int. J. Microgravity Sci. Appl. 32 (2015).
[38] Y. Sun, H. Muta, Y. Ohishi, Novel method for surface tension measurement: the drop-bounce method, Microgravity Sci. Technol. 33 (2021).
[39] W. Wien, Xxx. on the division of energy in the emission-spectrum of a black body, London Edinburgh Philos. Mag. J. Sci. 43 (262) (1897) 214–220.
[40] S. Krishnan, G. P. Hansen, R. H. Hauge, J. L. Margrave, Emissivities and optical constants of electromagnetically levitated liquid metals as functions of temperature and wavelength, Vol. 1, Humana Press, Totowa, NJ, 1990.
[41] W. Ranz, W. Marshall, Evaporation from drops., Chem. Eng. Prog. 48 (1952) 141–146.
[42] A. Bahadori, Chapter 4 - gas–liquid separators, in: A. Bahadori (Ed.), Natural Gas Processing, Gulf Professional Publishing, Boston, 2014, pp. 151–222.
[43] C. Tackes, Thermal analysis of undercooled metallic liquids by electromagnetic levitation drop calorimetry, Master's thesis, Iowa State University (2013).
[44] J. A. Lewis, W. H. Gauvin, Motion of particles entrained in a plasma jet, AIChE J. 19 (1973) 982–990.
[45] J. K. Fizdon, Melting of powder grains in a plasma flame, Int. J. Heat. Mass. Transf. 22 (1979) 749–761.
[46] Y. Lee, K. Hsu, E. Pfender, Modeling of particles injected into a dc plasma jet, in: Proceedings of the 5th International Symposium on Plasma Chemistry, Vol. 2, 1981, p. 795.
[47] X. Chen, Particle heating in a thermal plasma, Pure Appl. Chem. 60 (1988) 651–662.
[48] X. Chen, E. Pfender, Unsteady heating and radiation effects of small particles in a thermal plasma, Plasma Chem. Plasma Process 2 (1982) 293–316.
[49] X. Chen, E. Pfender, Heat transfer to a single particle exposed to a thermal plasma, Plasma Chem. Plasma Process 2 (1982) 185–212.
[50] X. Chen, E. Pfender, Effect of the knudsen number on heat transfer to a particle immersed into a thermal plasma, Plasma Chem. Plasma Process 3 (1983) 97–113.
[51] X. Chen, E. Pfender, Behavior of small particles in a thermal plasma flow, Plasma Chem. Plasma Process 3 (1983) 351–366.
[52] E. A. Brandes, G. B. Brook, Smithells Metals Reference Book, seventh Edition, Butterworth-Heinemann, 1998.
[53] I. Barin, O. Knacke, O. Kubaschewski, Thermochemical properties of inorganic substances, 1st Edition, Springer-Verlag Berlin Heidelberg, 1977.
[54] N. Wang, X. J. Han, B. Wei, Specific heat and thermodynamics properties of undercooled liquid cobalt, Appl. Phys. Lett. 80 (2001) 28–30.
[55] H. Hess, E. Kaschnitz, G. Pottlacher, Thermophysical properties of liquid cobalt, High Press. Res. 12 (1994) 29–42.
[56] V. N. Korobenko, O. A. Polyakova, A. I. Savvatimskii, Heat capacity of liquid hafnium from the melting point to the boiling point at atmospheric pressure, High Temperature 43 (2005) 38–44.
[57] S. Kang, D. H. Jeon, H. Yoo, J. T. Ishikawa, T. Okada, P. F. Paradis, G. W. Lee, Nanosized nucleus-supercooled liquid interfacial free energy and thermophysical properties of early and late transition liquid metals, Cryst. Growth Des. 14 (2014) 1103–1109.
[58] C. Cagran, G. Pottlacher, Thermophysical properties and normal spectral emittance of iridium up to 3500 k, Int. J. Thermophys. 28 (2007) 697–710.
[59] D. V. Minakov, M. A. Paramonov, P. R. Levashov, Thermophysical properties of liquid molybdenum in the near-critical region using quantum molecular dynamics, Phys. Rev. B 103 (2021) 184204.
[60] C. Cagran, B. Wilthan, G. Pottlacher, Normal spectral emissivity at a wavelength of 684.5 nm and thermophysical properties of solid and liquid molybdenum, Int. J. Thermophys. 25 (2004) 1551–1566.
[61] K. Boboridis, Thermophysical property measurements on niobium and titanium by a microsecond-resolution pulse-heating technique using high-speed laser polarimetry and radiation thermometry, Int. J. Thermophys 23 (2002) 277–291.
[62] A. Cezairliyan, J. L. McClure, Heat capacity and electrical resistivity of liquid niobium near its melting temperature, Int. J. Thermophys 8 (1987) 803–808.
[63] B. Wilthan, C. Cagran, G. Pottlacher, Combined dsc and pulse-heating measurements of electrical resistivity and enthalpy of tungsten, niobium, and titanium, Int. J. Theromphys. 26 (2005) 1017–1029.
[64] C. Brunner, C. Cagran, A. Seifter, G. Pottlacher, The normal spectral emissivity at a wavelength of 684.5 nm and thermophysical properties of liquid zirconium up to the end of the stable liquid phase, AIP Conf. Proc. 684 (2003) 771–776.
[65] Y. S. Touloukian, D. P. Witt, Thermal radiative properties, Vol. 7, IFI/ Plenum: New York and Washington, 1970.

Appendix A. Cooling curves of various transition metals

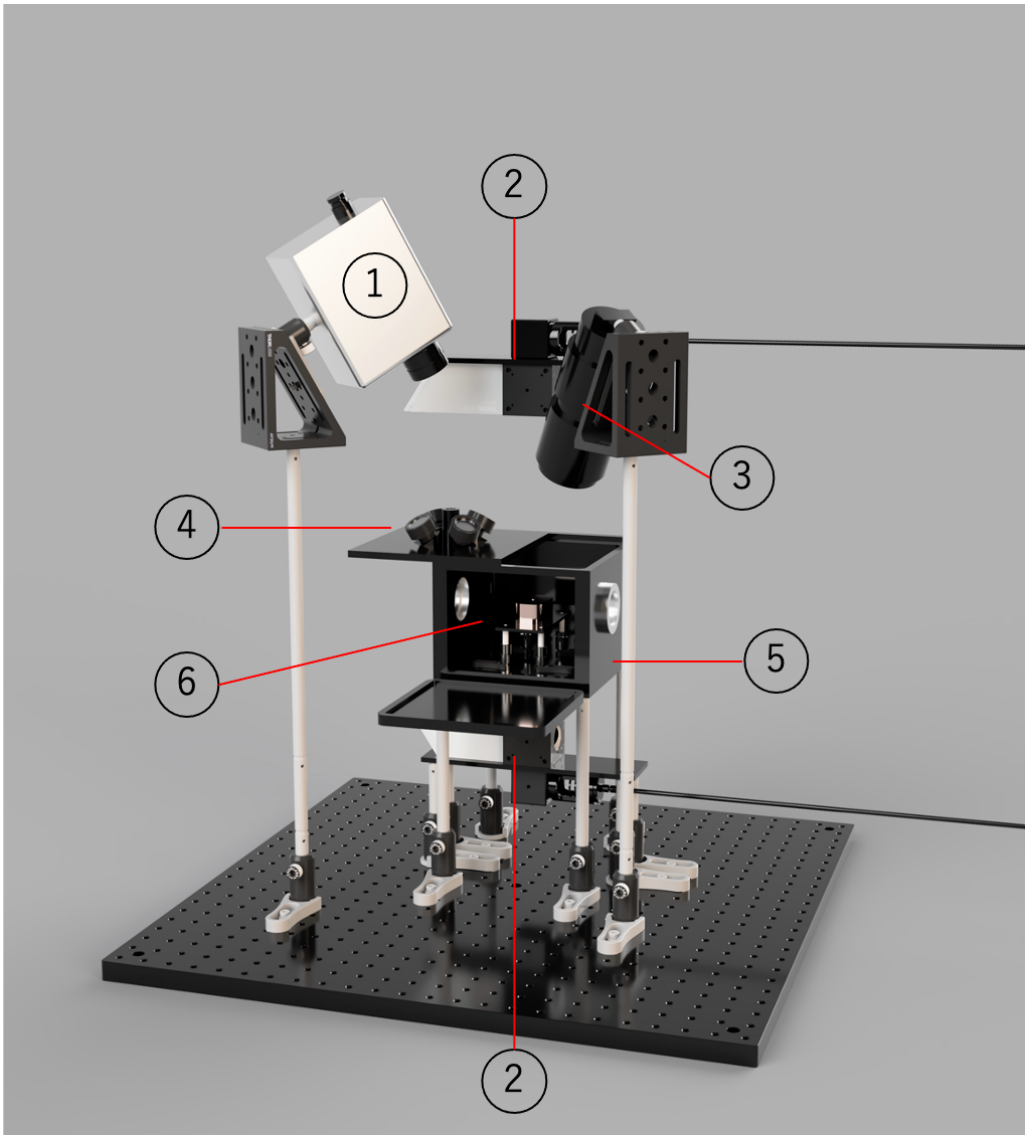

Figure 1: 3D rendering of the ADL setup used in this study. Some parts (e.g., laser units, cooling water, and levitation gas tubes) are not included for simplicity. (1) pyrometer, (2) upper and bottom heating lasers, (3) CCD camera, (4) sample chamber top cover plate with five slots for optical filters, (5) semi-sealed sample chamber, (6) location of levitation nozzle.

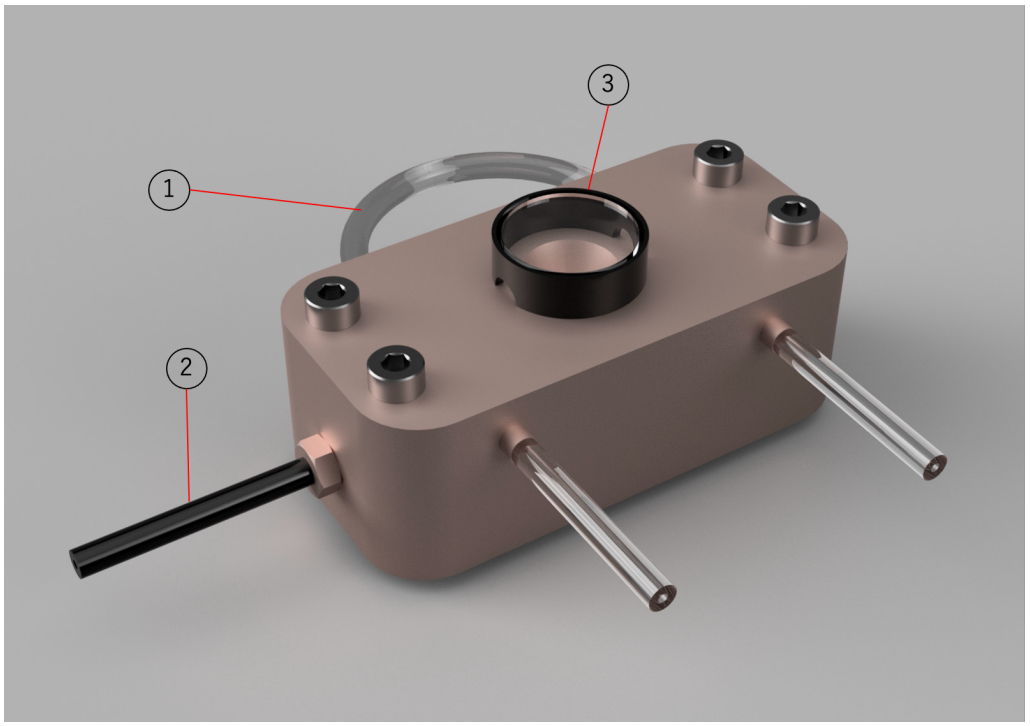

Figure 2: 3D rendering of the 1.4-mm-diameter conical nozzle used in this study. ① cooling water channel, ② levitation gas inlet, ③ top cover with sapphire window.

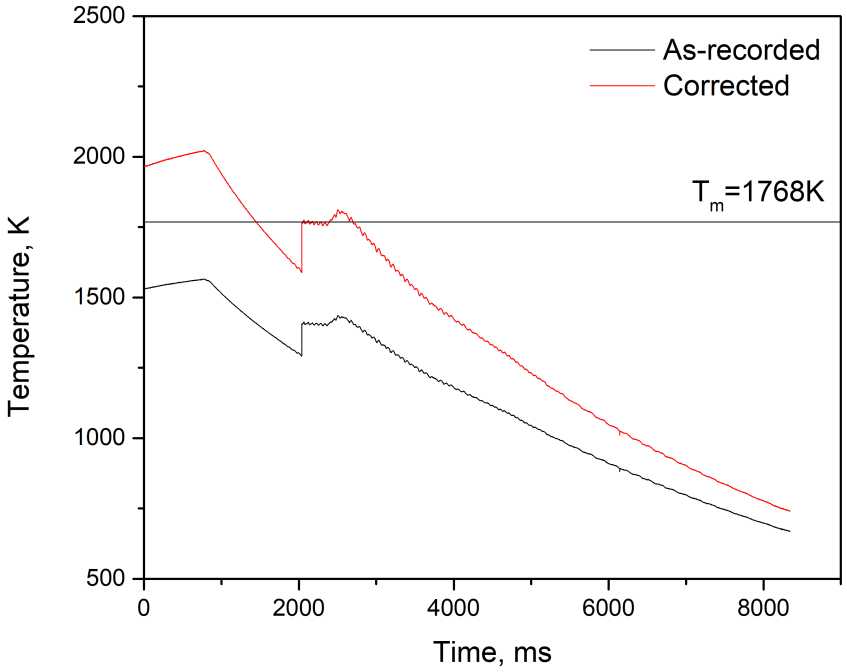

Figure 3: Comparison between an as-recorded and a corrected temperature curve for liquid cobalt cooled in argon gas.

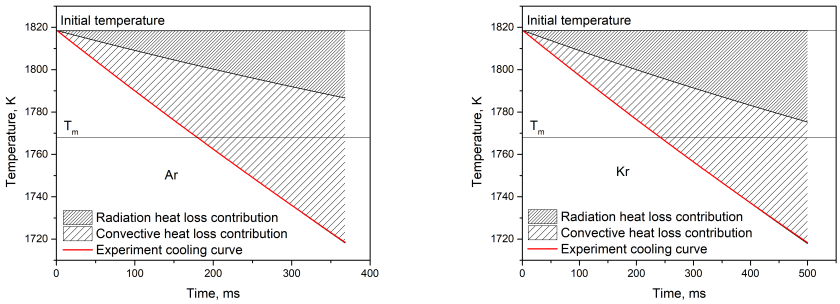

(a) Liquid cobalt cooled in argon gas.

(b) Liquid cobalt cooled in krypton gas.

Figure 4: Comparison between the experiment cooling curve and modeled heat loss behavior for a liquid cobalt sample cooled in (a) Ar and (b) Kr gas. The shaded regions represent the cumulative temperature decrease from the initial temperature through either the radiation heat loss or convection heat loss.

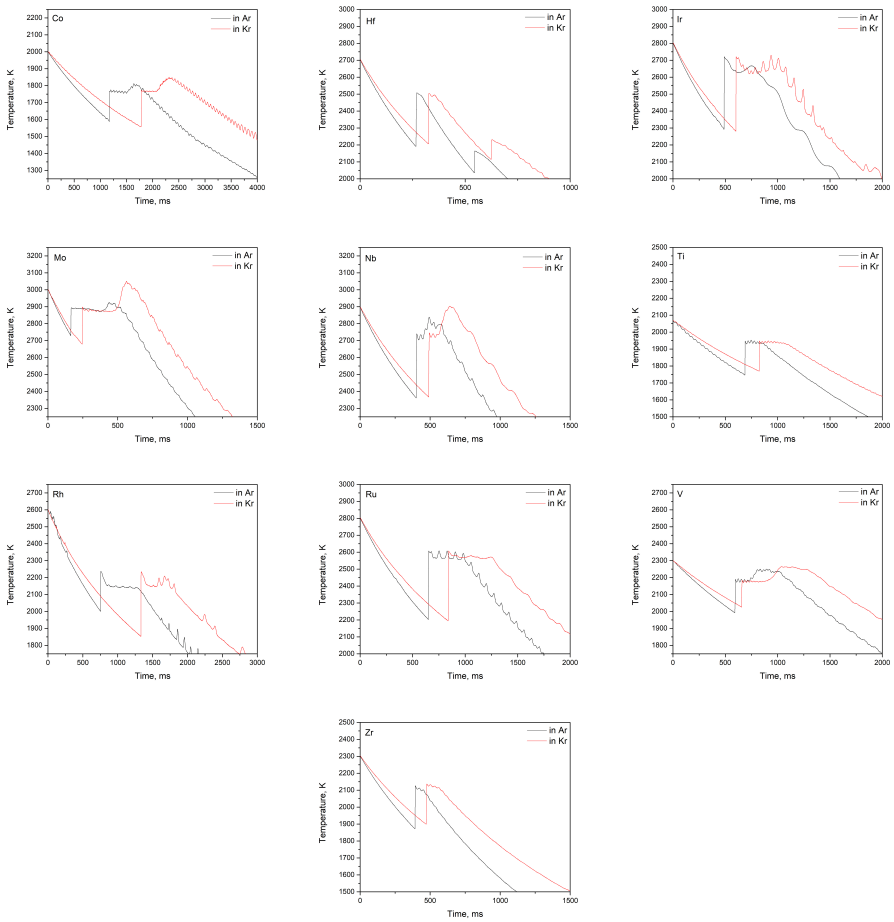

Figure A.5: Cooling curves of various transition metals (Co, Hf, Ir, Mo, Nb, Ti, Rh, Ru, V, and Zr) in argon (black) and krypton (red) gas. Two recalescence valleys were observed in Hf owing to Zr impurities.